Indian Journal of Pure & Applied Physics
Vol. 62, June 2024, pp. 503-509
DOI: 10.56042/ijpap.v62i6.7207

Structural and Magnetic Characterization of Nickel Nanoparticles Synthesized through Chemical Routes

Pinaki Laha[a]* & Rabindra Nath Gayen[b]

[a]Department of Physics, L.N.D. College, Motihari, B.R. Ambedkar Bihar University, Muzaffarpur, Bihar 845 401, India

[b]Department of Physics, Jadavpur University, Jadavpur, Kolkata 700 032, India

Received 8 December 2023; accepted 1 May 2024

This study presents the magnetic properties of clusters of ultrafine nickel nanoparticles synthesized through an aqueous chemical reduction technique. The morphology and microstructure of the synthesized nanostructures were characterized using scanning electron microscopy (SEM), transmission electron microscopy (TEM), and X-ray diffraction (XRD). The XRD results indicate that the nickel nanoparticles exhibit a polycrystalline face-centered cubic (FCC) structure with a particle size of 16 nm. The magnetic properties were investigated using a vibrating sample magnetometer (VSM) at different temperatures (80 K, 150 K, 300 K, and 400 K). The hysteresis loop confirms the ferromagnetic behaviour of the nickel nanoparticles. Samples grown under specific conditions exhibit a systematic change in saturation magnetization (Ms) and coercive field (H_C) with increasing temperature. The variation in saturation magnetization may be attributed to a decrease in particle size with temperature, resulting in an increased area-to-volume ratio.

The coercivity of the prepared nanoparticles demonstrates an increasing trend with decreasing temperature. Micromagnetic simulations using mumax3 were performed to explore the temperature dependency of nickel nanoparticles, and the results validate that coercivity decreases with an increase in temperature.

Keywords: Nanoparticle; Nickel; Chemical synthesis; Magnetic properties

1 Introduction

The unique response of magnetic nanoparticles to an external magnetic force is a distinctive feature that finds applications in various fields, including biomedicine and environmental treatment.In recent nanotechnology, nickel nanoparticles have garnered ample attention due to their unique chemical, physical, and magnetic properties[1-4]. NiNPs have potential applications in various technological arenas, including battery manufacturing, catalysis, the printing industry, enhanced pseudo-capacitance, the textile industry, field-modulated gratings and optical switches, direct control of biomolecules through the magnetic force of NiNPs, and the adsorption of basic yellow dyes[5-11]. Nickel nanoparticles are unique among all other magnetic nanoparticles and are commonly used as propellants, catalysts in reactions, and sintering additives in plastics, coatings, and fibers[11,12]. Nickel (Ni) is more cost-effective than most metals used for catalytic activity, antimicrobial activity, cytotoxicity, and antioxidant applications due to its abundance in the Earth's crust[13-15]. The electrical conductivity of nickel nanoparticles permits for their versatile use in numerous applications[16]. NiNPs can be used as nano ferro fluids in ultra-high purity, passivated, coated, and distributed forms[17]. The tuning of magnetic interaction in the nanoparticle structure by the controlling of the size and shape distribution is of great importance. In the last decade, we have witnessed significant advancements in the application of magnetic nanoparticles in various technological domains. Non-toxic, biocompatible magnetic nanoparticles are commonly used for magnetic hyperthermia, such as Ni, Fe, Co, Gd etc. Theseferromagnetic nanoparticles exhibit high magnetic anisotropy and high coercivity (Hc) compared to the bulk material. However, this high coercive field is not suitable for magnetic hyperthermia[11]. Therefore, it becomes essential to explore methods to reduce this coercive field. It is well established that the magnetic properties of surfaces and nanostructures can differ significantly from those of the bulk material. Nickel nanoparticles (NiNPs) have gained considerable technological importance owing to their intriguing electrical, chemical, and magnetic properties, coupled with good

*Corresponding author: (E-mail: lahapinaki007@gmail.com)

thermal stability. The preparation of magnetic nanoparticles involves various chemical and physical methods, including the polyol process, organometallic decomposition, and chemical reduction methods.Among these synthesis methods, the chemical reduction method stands out as a suitable technique for producing ferromagnetic metal particles with quasi-spherical or rod-like shapes and a narrow size distribution, depending on the synthesis conditions. The primary advantages of the chemical synthesis process include the simplicity of preparation, the flexibility of the experimental procedure, and the cost-effectiveness of the technical apparatus.

This paper aims to compare the properties and phenomena of NiNPs at different temperatures, specifically in the form of fine particles with similar sizes and very similar crystal structures.

In this research article, we present the synthesis of nickel nanoparticles using the aqueous chemical reduction technique. The synthesized nickel nanoparticles were comprehensively characterized through XRD, SEM, EDX, and TEM analyses. Magnetic properties of the prepared nickel nanoparticles were systematically investigated using a vibrating sample magnetometer (VSM) at temperatures of 80 K, 150 K, 300 K, and 400 K.

For magnetic hyperthermia application, both single- and multi-domain ferromagnetic nanostructures have recently garnered significant attention due to their potential to enhance heating efficiency through hysteresis losses. Various strategies have been employed to adjust hysteresis properties with the goal of augmenting the relative heating contribution. The results provide a detailed examination of the magnetic behaviour of nickel nanoparticles in the form of nano-sized particles, revealing qualitatively distinct magnetic behaviours and quantitatively different properties, such as magnetic anisotropy and coercivity, with varying temperatures. Micromagnetic simulations, carried out using mumax3 software, offer valuable insights into the magnetization processes of Nickel NPs, contributing to a comprehensive understanding of their behaviour under different temperature conditions.

2 Synthesis and Characterization

Nickel nanoparticles were synthesized by the chemical reduction method with hydrazine hydrate acting as the reducing agent at room temperature. For first aqueous solution, 10.69 gm of nickel chloride ($NiCl_2.6H_2O$) were dissolved using de-ionized water. In a separate beaker the second solution was prepared by dissolving 4 gm NaOH in de-ionized water and then adding 45.054 gm hydrazine hydrate. Then the second solution was mixed with the first solution. The combined solution turns into royal blue colour and it was stirred for five minutes and the pH value of the solution was 12.5. For nickel nanoparticles protection stabilizer polyvinylpyrrolidone (PVP) was introduced into the NaOH, hydrazine solution and the solution were stirred at room temperature. Then the solution is sonicated for 30 minutes. The solution initially became grey and after some time black precipitate found at the bottom of the beaker. A fine precipitate was obtained and filtered, then washed three times with de-ionized water, after that water was removed with acetone. Acetone was used as a dehydrating agent since it has a high solubility for water but not for the metal salts involved.

The crystallographic structure, composition, and particle size of the nanocrystalline, cubic copper ferrite thus produced were studied using X-ray diffraction (XRD; PANalytical X'Pert PRO), scanning electron microscope (SEM; Helios NanoLab, FEI), energy dispersive x-ray spectrometer (EDX; Helios NanoLab, FEI), and transmission electron microscope (TEM; Helios NanoLab, FEI). The magnetization (M) versus the applied magnetic field (H) was measured using vibrating sample magnetometer (VSM; Lakeshore model 7407). The magnetic field (up to 10kOe) is applied during the measurements.

3 Results and Discussion

3.1 XRD Analysis

X-Ray diffraction was used to analyze the structure and particle size of the powders. Fig. 1 shows a typical XRD pattern of the Ni powder sample after sonication, filtration, and drying. The five characteristic peaks for nickel 2θ = 44.45°, 51.71°, and 76.41° corresponding to Miller indices (111), (200), and (220) respectively, were observed, indicating that the resulting powders are face centered cubic (*fcc*) nickel (PDF #04-0850). As seen from the XRD plot, the (111) reflection is the highest intensity for the peaks. The observed XRD parameters are is in well agreement with the standard JCPDS card No. 04-0850, the pattern matches a random powder arrangement for nickel.

The average particle size (D) was determined based on the diffraction peak using Debye – Scherrer's equation: $D = k\lambda/L\cos\theta$

where, λ is the wavelength of the Cu-Kα radiation, θ is the diffraction angle, k is the Scherrer constant which takes the value of 0.97 for spherical crystals with cubic symmetry[17], and L is the FWHM of the diffraction line corrected for the instrumental broadening. The average crystallite size calculated by using above equation is ~16 nm. This is indicating the nanocrystalline nature of the Nickel nanoparticles.

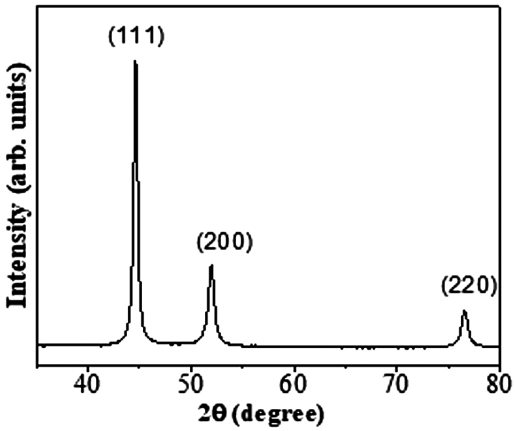

Fig. 1 — XRD pattern of nickel nanoparticles

3.2 SEM Analysis

Scanning electron microscopy (SEM) was employed to determine whether the nanoparticles fell within the nanometer size range and exhibited a spherical shape. In Fig. 2(a), spherical nickel nanoparticles coated with PVP, forming weak agglomerates, were observed. The SEM images clearly indicate that the nanoparticles are nearly uniformly spherical in shape and possess a small diameter.

3.3 EDX Analysis

Compositional analysis of the nickelnanoparticles was performed by Energy Dispersive X-ray (EDX) attached with SEM and is shown in Fig. 2(d). To confirm the uniformity of composition we performed spot EDX analysis at different points of the nanoparticle. The EDX spectrum confirms the chemical purity of the nanoparticles. The composition of the sample at room temperature was determined using EDX on various sample regions. The results show that the samples consisted of ~ 98% pure metallic nickel on the basis of the NiL and NiK peaks at ~ 0.8, ~ 7.5 keV and ~ 8.25 keV in the EDX spectra. The detected silicon arises from the use of the silicon substrate, and the detected oxygen is attributed

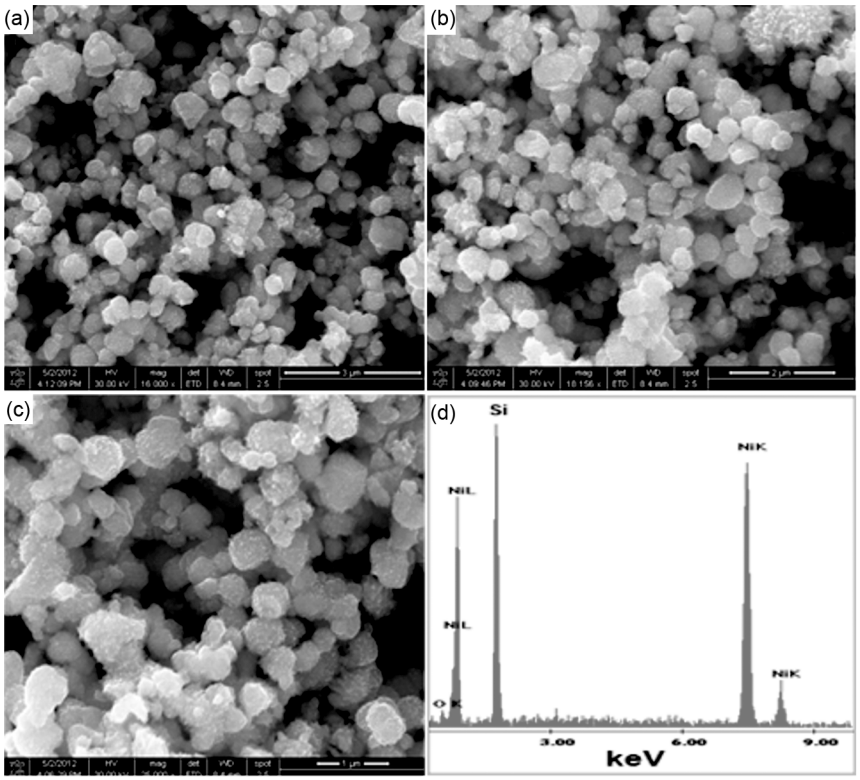

Fig. 2 — (a), (b), (c) SEM images of nickel nanoparticles with different magnifications (d) EDX spectra of nickel nanoparticles

to the residual solvent or to partial particle oxidation during sample preparation for microscopic analysis. No other elements were detected in the EDX spectra.

3.4 TEM Analysis

Figures 3(a & b) shows the TEM images of nickelnanoparticles. The nanoparticles dispersed in isopropyle alcohol were drop casted on Cu mesh grid and dried in ambient to prepare for measurement in Transmission Electron Microscope (TEM; Helios NanoLab, FEI). It shows the particle size and shape distribution of the synthesized nanoparticles coated with PVP which have an average size of 16 nm. The bright field and dark field images indicate that the samples have a large polymer region surrounding the NiNPs. The dark field images suggest the presence of crystalline NiNPs. The images reveal that the NiNPs are solid, spherical, and agglomerated. Large spherical nanoparticles of pure Ni are composed of smaller crystalline NiNPs. Small particles tend to aggregate into large nanoparticles through van der Waals attraction.Selected area electron diffraction (SAED) pattern reveals that nickel nanoparticles were polycrystalline fcc structure.

3.5 M-H Loop Analysis

Figure 4 shows the Magnetization (M) vs. applied field (H) curves of Nickel nanoparticle for four different temperatures 80 K, 150 K, 300 K and 400 K. It can be seen that Nickel nanoparticles showed ferromagnetic character with the saturation magnetization are 36.9, 37.9, 39 and 41 emu/g, respectively. The M–H curves clearly shows that the all-nano products are ferromagnetic character and difference in the value of the saturation magnetization. Coercivity value has been derived from the M-H loops and presented in Fig. 5. The dependence of coercivity and saturation magnetization is presented in the Fig. 6 for 80 K, 150 K, 300 K and 400 K. Result shows that coercive value decreases with temperature and saturation magnetization value increases with temperature.

In an infinitely large ferromagnetic system, the saturation magnetization, when well below the Curie temperature, conforms to the Bloch law[17], expressed as: $M_S(T) = M_S(0)[1-BT^{3/2}]$, where B is the Bloch constant related with the structure of the material.

However, it has been established that at the nano scale, finite size effects lead to modifications in the spin wave spectrum, and these modifications can be characterized by a power-law relationship with temperature 'T' expressed as: $M_S(T) \alpha T^{\alpha}$. In this power-law expression, 'α' defines the influence of finite

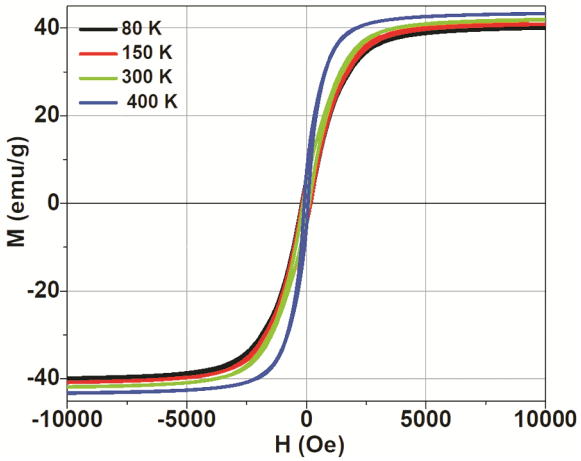

Fig. 4 — M-H loop of nickel nanoparticles with different temperature (a) 80 K, (b) 150 K, (c) 300 K and (d) 400 K

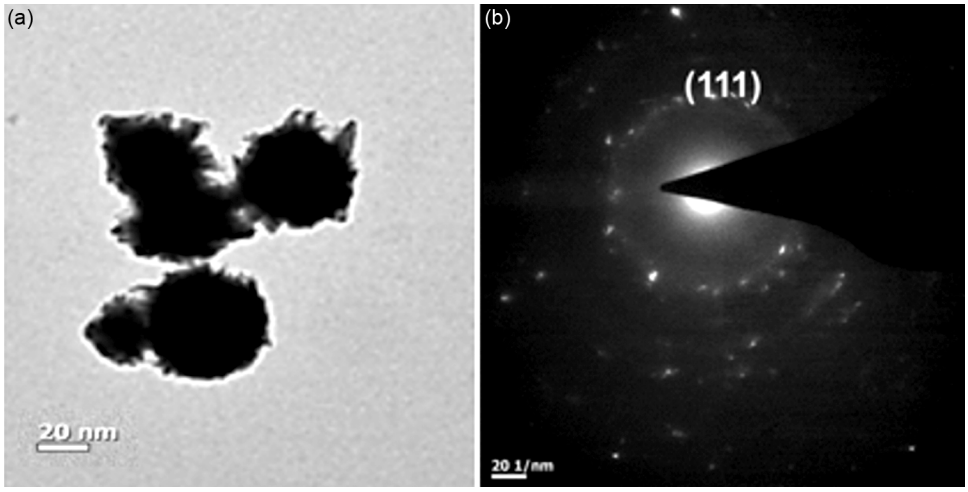

Fig. 3 — TEM images of nickel nanoparticles coated with PVP

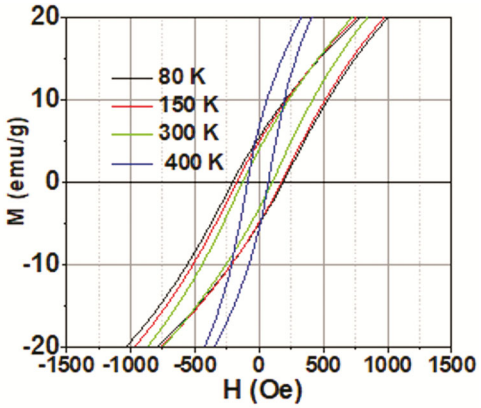

Fig. 5 — Temperature dependence of the coercivity H_C and M_S of nickel nanoparticles with different temperature

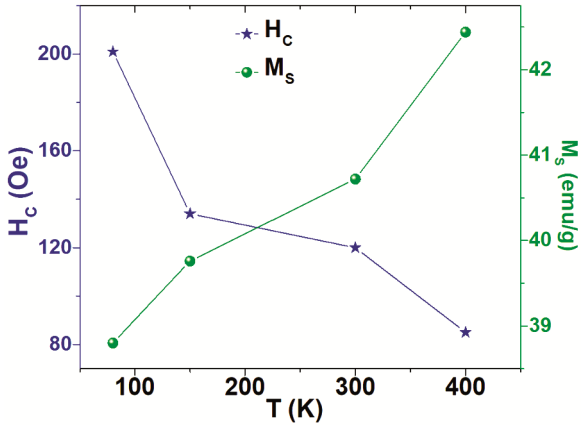

Fig. 6 — Expanded view of M-H loop of nickel nanoparticles with different temperature (a) 80 K, (b) 150 K, (c) 300 K (d) 400 K

size effects on the saturation magnetization at the nanoscale[13,17-19]. The reduction of M_S value is probably due to the random surface spins. The observed phenomena can be attributed to two underlying mechanisms: the redistribution of cations within the particle's core and the presence of spin disorder in the surface shell. This behavior is linked to what is commonly referred to as the surface effect, where it becomes evident that beyond the well-ordered core region, the surface layers exhibit a state of fixed disorder, effectively forming a magnetically inactive layer. The surface energy density, increases steadily with nanoparticle diameter, eventually approaching bulk levels, rendering fcc metallic nanoparticles similar to liquid droplets[20,21]. As the particle size decreases, a larger number of atoms remain on the surface, and these atoms do not engage in exchange coupling. Consequently, this leads to a decrease in magnetic induction. This effect becomes particularly pronounced when the particle sizes are exceedingly small.

In theory, the cohesive energy (En) of free-standing nanoparticles with random shapes can be described using the formula[22]:

$$E_n = E_b\left(1 - \frac{6\mu}{n^{1/3}C^{2/3}\pi k^2}\right) \quad \ldots (1)$$

Here, E_b represents the cohesive energy of the corresponding bulk materials, μ is the shape factor, n is the atomic number of the nanocrystals, C is the atomic number of the structural unit cell, and k is the ratio between the equivalent atomic radius and the lattice parameter.

Taking into consideration that the Curie Temperature (T_C) is proportional to the cohesive energy, the Curie temperature (T_{Cn}) of nanoparticles can be expressed as:

$$T_{Cn} = T_{Cb}\left(1 - \frac{6\mu}{n^{1/3}C^{2/3}\pi k^2}\right) \quad \ldots (2)$$

where T_{Cb} denotes the Curie temperature of bulk materials. For spherical nanoparticles, the atomic number n can be expressed as

$$n = \frac{\rho\frac{4}{3}\pi\left(\frac{D}{2}\right)^3}{M}N_A \quad \ldots (3)$$

where ρ denotes the density of materials, D denotes the size of nanoparticles, M is the molar mass of matter, N_A is the Avogadro constant. In this system, spherical Nickel nanoparticles with *fcc* structure, the μ, C and k are 0.806, 4 and $\frac{\sqrt{2}}{4}$ and ρ = 8.908 g/cm^3, M = 58.69 g/mol, N_A = 6.023 ×10^{23} mol^{-1}, T_{Cb} = 358 °C respectively and the putting the values in Eq. (2) and (3)[22-24]. The Curie temperature T_C of Nickel nanoparticles with particle size D = 16 nm can be expressed as,

$$T_C = 358 - \frac{482.38}{D} \quad \ldots (4)$$

The value of Curie temperature (T_C) of Nickel nanoparticle is 329.63 °C which is almost equal to the reported value.The Curie temperature (Tc) of nickel nanoparticles can vary depending on factors like the size, shape, and surrounding environment. However, in bulk nickel, the Curie temperature is approximately 358 °C or 631 K. In nanoscale nickel particles, the Curie temperature may be altered due to size effects and surface interactions.

The effective anisotropy constant (Keff) for Nickel nanoparticles can be determined through the Law of Approach to Saturation (LAS). This law describes the relationship between magnetization (M) and the applied magnetic field (H) in the high magnetic field range (H >>Hc). In accordance with

LAS, the magnetization near saturation (Ms) can be expressed as[24,25],

$$M = M_S\left(1 - \frac{b}{H^2}\right) \quad \ldots (5)$$

where the parameter b is related with the effective anisotropy constant as[25]:

$$K_{eff} = \mu_0 M_S \sqrt{\frac{15b}{4}} \quad \ldots (6)$$

For the calculation of K_{eff} value, using the experimental hysteresis loop a graph can be plotted M as a function of $\frac{1}{H^2}$ by the Eq. 5. From Eq. 6, we can calculate K_{eff} value using the obtained value of b from the M versus $\frac{1}{H^2}$ graph. Surface effect leads to large anisotropy value in magnetic nanoparticles[26]. The interaction between the core and surface spins leads to the large anisotropy and exchange bias effects. Generally, magnetic nanoparticles show a higher anisotropy value compared to their bulk counterpart. The calculated value of magnetic anisotropy constant of nickel nanoparticles is 4.73 × 10^5 erg cm^{-3}, 4× 10^5 erg cm^{-3}, 4.46 × 10^5 erg cm^{-3} and 4.11 × 10^5 erg cm^{-3} at 80 K, 150 K, 300 K, and 400 K respectively which is larger than that of bulk nickel (2.36 × 10^5 erg cm^{-3})[27].

When the squareness (Mr/Ms) value is greater than or equal to 0.5, it is indicative of a single-domain structure in nanoparticles. However, in this study, the squareness value is significantly less than 0.5. This result suggests that the nickel nanoparticles exhibit a multi-domain structure and possess uniaxial anisotropy[28].

The magnetic properties such as the saturation magnetization (Ms), and coercivity (Hc) are extracted from the hysteresis loops. The magnetic moment (μ_B) per atom in Bohr magneton is calculated using the following equation[28],

$$\mu_B = MW \times \frac{M_S}{5585} \quad \ldots (7)$$

where, MW is the molecular weight of Nickel. The Bohr magneton (μ_B) values are 0.408, 0.418, 0.428 and 0.446 at 80 K, 150 K, 300 K and 400 K.

3.6 Micromagnetic Simulation Results

Figure 7 shows the Magnetization (M) vs. B (Tesla) curves of Nickel nanoparticles at four different temperatures: 0 K, 300 K, 400 K, and 700 K. From Fig. 7, it is evident that Nickel nanoparticles exhibit a ferromagnetic character with variations in the coercivity values. The coercivity value steadily decreases with increasing temperature. The temperature effect is introduced in mumax3[29] as a fluctuating thermal field, based on the description given by Brown[30]. This thermal field introduces a random oscillation term to the LLG effective field, which changes at each time step. It is noteworthy that even a slight increase in temperature significantly reduces the coercivity values compared to the case at 0 K. As the temperature further increases, the coercivity continues to decrease due to the random oscillations introduced by the thermal field. The reduction in coercivity is expected when adding the thermal field since it makes it easier to "pull" the magnetization out of its previous equilibrium direction, which is defined by the ordered core anisotropy easy axis (lying along the x-direction in our simulations). At higher temperatures, the spins struggle to remain fairly parallel to each other due to the stronger oscillations caused by the thermal field.

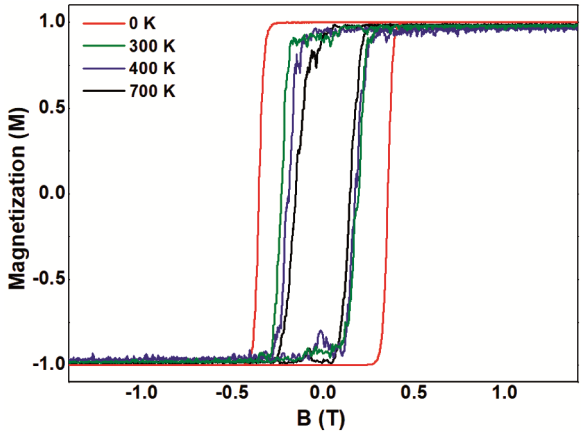

Fig. 7 — Micromagnetic simulation results of hysteresis loop of nickel nanoparticles with different temperature (a) 0 K, (b) 300 K, (c) 400 K and (d) 700 K

4 Conclusion

We have successfully synthesized nickel nanoparticles using the aqueous chemical reduction method. This approach has enabled us to produce high-quality nickel nanoparticles with controlled sizes and excellent magnetic properties. Our investigation has revealed a strong correlation between the structural analysis, surface morphology, and magnetic characteristics of these nanoparticles. In addition, we conducted a systematic examination of the temperature-dependent magnetic properties of spherical nickel nanoparticles, employing both experimental measurements and theoretical calculations. Our findings indicate that saturation

magnetization increases monotonously as temperature rises, while coercivity consistently decreases. Importantly, our calculated results are in excellent agreement with the experimental data. Moreover, as the particle size decreases, the surface-to-volume ratio of the nickel nanoparticles increases, resulting in a higher percentage of magnetically inactive layers. Furthermore, our micromagnetic simulations have qualitatively aligned with the experimental outcomes.

References

1 Paramo L A, Feregrino-Perez A A, Guevara R, Mendoza S & Esquivel K, *Nanomaterials*, 10 (2020) 1654.
2 Magaye R & Zhao J, *Environ Toxicol Pharmacol*, 34 (2012) 644.
3 Bibi I, Kamal S, Ahmed A, Iqbal M, Nouren S & Jilani K, *et al*., *Int J Biol Macromol*, 1037 (2017) 83.
4 Cheng Y, Guo M, Zhai M, Yu Y & Hu J, *J Nanosci Nanotechnol*, 20 (2020) 2402.
5 Fattah A R A, Majdi T, Abdalla A M, Ghosh S & Puri I K, *ACS Appl Mater Interfaces*, 8 (2016) 1589.
6 Jiao M, Yao Y, Pastel G, Li T, Liang Z, Xie H, *et al.*, *Nanoscale*, 11 (2019) 6174.
7 Ni H, Zhu J, Wang Z, Lv H, Su Y & Zhang X, *Rev Adv Mater Sci*, 58 (2019) 98.
8 Mary A P R, Suchand C S S, Narayanan T N, Philip R, Moloney P, Ajayan P M, *et al*., *Materials*, 22 (2011) 375702.
9 Barsan M M, Enache T A, Preda N, Stan G, Apostol N G, Matei E, *et al*., *ACS Appl Mater Interfaces*, 11 (2019) 19867.
10 Kiran S, Rafique M A, Iqbal S, Nosheen S, Naz S & Rasheed A, *Environ Sci Pollut Res*, 27 (2020) 32998.
11 Apostolova I & Wesselinowa J M, *Phys Status Solidi B*, 246 (2009) 1925.
12 Hill D, Barron A R & Alexander S, *J Colloid Interface Sci*, 555 (2019) 323.
13 Bian Z, Das S, Wai M H, Hongmanorom P & Kawi S, *Chem Phys Chem*, 18 (2017) 3117.
14 Tailor G, Chaudhary J, Jandu S, Mehta C, Yadav M & Verma D, *Res Chem*, 6 (2023) 101195.
15 Sana S S, Singh R P, Sharma M, Srivastava A K, Manchanda G, Rai A R & Zhang Z J, 22 (2021) 808.
16 A Sagasti, V Palomares, J M Porro, I Orue, M B Sanchez-Ilarduya, A C Lopes, *et al*., *Materials*, 13 (2019) 57.
17 Bloch F, *Z Phys*, 61 (1930) 206.
18 Wang D, Jia Y, He Y, Wang L, Fan J, Xie H, *et al.*, *J Colloid Interface Sci*, 557 (2019). 266.
19 Obaidat I M, Issa B & Haik Y, *Nanomaterials (Basel)*, 5 (2015) 63.
20 Goyal M & Gupta B R K, *Pramana – J Phys*, 90 (2018) 80.
21 Samsonov V M, Shcherbakov L M, Novoselov A R & Lebedev A V, *Colloid Surf A: Phys Eng Asp*, 160 (1999) 117.
22 Xie D, Wang M P & Cao L F, *Phys Stat Sol (b)*, 242 (2005) R76.
23 Askeland D R & Phule P P, The Science and Engineering of Materials, New York: Thomson Learning Inc; (2003).
24 Web elements periodic table. http://www.webelements.com/nickel/.
25 Mameli V, Musinu A, Ardu A, Ennas G, Peddis D, Niznansky D, Sangregorio C, Innocenti C, Thanh N T K & Cannas C, *Nanoscale*, 8 (2016) 10124.
26 Nemati Z, Salili S M, Alonso J, Ataie A, Das R, Phan M H & Srikanth H, *J Alloys Compd*, 714 (2017) 709.
27 Hou Y & Gao S, *J Mater Chem*, 13 (2003) 1510.
28 Shinde V S & Dahotre S G, *Cerâmica*, 67 (2021) 301.
29 Vansteenkiste A, Leliaert J, Dvornik M, Helsen M, Garcia-Sanchez F, Waeyenberge B Van, *AIP Adv*, 4 (2014) 107133.
30 Brown W F, J Appl Phys, 34 (1963) 1319.